scientific reports

Check for updates

OPEN

Freeze-thaw seasonal variations and environmental controls of CO_2 and CH_4 diffusive emissions from reservoirs in the upper Yellow River

Chen Li[1,2], Wei Wu[1,2]✉, Hang Chen[1], Lei Ren[1] & Xiao Kang[1]

Reservoirs are significant sources of atmospheric carbon greenhouse gas (carbon dioxide [CO_2] and methane [CH_4]) emissions. This study analysed the seasonal emission patterns of CO_2 and CH_4 concentrations and diffusive fluxes from water bodies, along with the associated environmental controls, in the three large reservoirs of the upper Yellow River on the Tibetan Plateau. The results indicated that the soil thawing period represented a critical window for carbon greenhouse gas emissions from reservoirs (CO_2: 239.3 ± 94.4 mmol m^{-2} d^{-1} and CH_4: 201.1 ± 366.6 mmol m^{-2} d^{-1}). Emissions of these gases from reservoirs were predominantly driven by photodegradation of organic carbon during the soil freezing period, whereas anaerobic respiration by microorganisms was the primary process during the soil thawing period, supplemented by photodegradation. CO_2 emissions from reservoirs were driven primarily by natural environmental pressures, particularly the alpine climate and high altitude of the plateau region. Precipitation and altitude were the main factors influencing the carbon input from terrestrial sources, whereas dissolved oxygen and chlorophyll-a predominantly governed the metabolism of carbon from endogenous sources. CH_4 emissions from reservoirs were influenced primarily by anthropogenic environmental pressures, including reservoir siltation and the confluence of tributaries characterized by high pollutant loads. Ammonia nitrogen served as a critical limiting factor for CH_4 emissions, which, along with dissolved oxygen, pH, and oxidation–reduction potential, collectively affect CH_4 releases. These findings enhance the understanding of the balance of greenhouse gas carbon emissions in reservoirs on the Tibetan Plateau and provide a scientific basis and theoretical support for greenhouse gas emission reduction in this region.

Keywords CO_2 and CH_4 emissions, Seasonal variations, Environmental controls, Large reservoirs, Upper Yellow River

Inland water bodies (rivers, streams, lakes, and reservoirs) play a key role in the global transport, transformation, and storage of carbon as an important component of the land-ocean aquatic continuum[1,2]. Recent studies have shown that inland waters are an important source of greenhouse gases (GHGs) in the atmosphere[3–5]. The carbon flux leaving terrestrial ecosystems (5.1 Pg C yr^{-1}) is much higher than that ending up in the oceans (0.9 Pg C yr^{-1}), suggesting that most of the carbon flowing through inland waters is lost as emissions at the water-air interface[5–7]. The global annual fluxes of CO_2 and CH_4 emitted to the atmosphere from inland waters are 5.5 Pg C $yr^{-1}$and 100 Tg C yr^{-1}, respectively[8]. Of this, about 40% of the carbon is buried in reservoir sediments[9].

With increasing anthropogenic activities such as damming of rivers, land and water carbon cycle processes have been altered, leading to more complex dynamics of carbon emissions from water bodies[10,11]. Carbon emissions from reservoirs are influenced by a multitude of environmental factors, making them strongly complex and variable in time and space[2,5,12]which are characterised by climate influences[13]hydrological regulation[14]geographic and historical features[15]biogeochemical cycles[16]anthropogenic disturbances[17,18]and ecosystem feedbacks[19]among other key process interactions. For instance, global studies indicate that the size and distribution of reservoirs, along with diurnal, freeze-thaw, and seasonal temperature variations, as well as eco-climatic zones, significantly affect the spatial and temporal patterns of CH_4 emissions[19–21]. The study by Deemer and Holgerson (2021)[22] compared the different driving mechanisms of CH_4 emissions from lakes

[1]State Key Laboratory of Water Engineering Ecology and Environment in Arid Area, Xi'an University of Technology, Xi'an 710048, China. [2]Chen Li and Wei Wu authors equally contributed to this work. ✉email: wuwei@xaut.edu.cn

and reservoirs, and found that lakes are mainly driven by morphological characteristics such as surface area and maximum depth, whereas reservoirs are mainly driven by autochthonous productivity such as Chl-a. The productivity of CH_4 emissions from lakes and reservoirs is mainly driven by surface area and maximum depth. Among them, productivity drives CH_4 ebullitive flux, while morphological characteristics and water body type jointly regulate CH_4 diffusion flux. Research on three temperate gradient reservoirs in northern China, which exhibit varying trophic levels and polymorphisms, revealed that CH_4 discharge is regulated by distinct bottom mechanisms, with water depth and productivity co-regulating CH_4 discharge[23]. Although the Revelle factor and hydraulic retention time of non-karst reservoirs are lower than those of karst reservoirs, CO_2 emissions are 3.5 times higher in non-karst reservoirs, highlighting the impact of different geological environments on GHG emissions from reservoirs[24].

CO_2 and CH_4 emissions from reservoirs involve multiple interfaces such as water-land, sediment-water, and water-air, as well as multiple processes such as endogenous production and exogenous input. When the partial pressure of CO_2 and CH_4 in water exceeds the equilibrium partial pressure in the atmosphere, CO_2 and CH_4 are released to the atmosphere at the water-air interface[25]. The sources of CO_2 and CH_4 in water bodies are classified into endogenous production and exogenous input[26]. Among them, endogenous sources are CO_2 production from microbial respiration, degradation and mineralisation of organic matter in the water column and sediments[27]and CH_4 production from anaerobic decomposition of organic matter in sediments[28]. Exogenous sources are lateral inputs of CO_2 and CH_4 to the water column from soil respiration in the terrestrial domain[29]. The dynamics of CO_2 and CH_4 concentrations are a result of the balance between their sources and consumption[30,31]and any environmental factors directly or indirectly involved in these processes could potentially affect CO_2 and CH_4 emissions[32]. For example, elevated water temperatures provide suitable conditions for the biological metabolism of carbon in the water column[33]. Anoxic environment favours photosynthetic carbon sequestration within the water column[34]inhibiting CO_2 production but promoting CH_4 producing activities of anaerobic microorganisms[35]. Changes in nutrient concentrations not only regulate the primary production and metabolic processes of phytoplankton, but also provide sufficient substrate for sediment microorganisms, which affects CO_2 and CH_4 production and release in reservoirs[30,36,37]. Precipitation brings exogenous organic matter into water bodies, changing the balance between primary production and organic matter consumption and decomposition in water bodies, indirectly affecting carbon emissions from reservoirs[38,39]. Therefore, it is important to understand the key factors influencing and regulating CO_2 and CH_4 emissions from reservoirs, especially in environmentally specific and sensitive areas.

The upper Yellow River (UYR), situated in the northeastern region of the Tibetan Plateau, which is characterized by a typical continental alpine climate. This area is a crucial source of flow and water conservation within the Yellow River basin, is highly sensitive to climate change and is ecologically fragile. The combined effects of climate change and human activities have resulted in a general degradation of the ecosystem in the UYR, as evidenced by phenomena such as glacier retreat, permafrost thawing, land degradation, and salinization. Future climate change is anticipated to exacerbate the warming and drying trends in this region, thereby increasing the risk of further ecosystem degradation. However, recent studies have revealed that the inland waters of the Tibetan Plateau may represent a significant source of carbon emissions to the atmosphere[6,40–42]. This phenomenon is largely attributed to climate warming, which has resulted in a 14.3% increase in soil respiration rates across the Tibetan Plateau[43]. Additionally, freeze–thaw cycles occurring on seasonally frozen ground facilitate the transfer of substantial amounts of terrestrial carbon into inland waters, leading to the rapid release of weathered inorganic carbon and unstable soil organic carbon, thereby influencing carbon emissions from these water bodies[44,45]. Moreover, the dynamic characteristics and drivers of the CO_2 and CH_4 emissions from inland waters in the region vary in response to different freeze–thaw periods. For example, the mean annual emission flux of CO_2 from rivers in the headwater region of the Qilian Mountains was measured at 0.45 (0.03–1.6) kg CO_2 m^{-2} yr^{-1}, with winter emissions being three times higher than those observed in other seasons. Seasonal variations in CO_2 emissions are influenced primarily by factors such as chemical weathering, photosynthesis, carbonate balance, and groundwater[46]. Additionally, subglacial environments might serve as potential sources of CH_4 due to their anaerobic conditions[6]. Cold-tolerant methanogenic archaea have been identified in glaciers and highland rivers[47]. In rivers fed by glacial meltwater, the CH_4 concentrations were observed to be supersaturated, with emission rates ranging from 0.04 to 735 mmol m^{-2} d^{-1}, and ebullitive releases accounted for 79% of the total flux[48]. This suggested that the inland waters of the Tibetan Plateau might exhibit higher total CH_4 fluxes and that climate warming could exacerbate CH_4 releases[49]. However, few studies have been conducted in this environmentally specific and sensitive region because of the difficulty associated with field sampling[6].

To enhance the understanding of carbon emissions from reservoirs on the Tibetan Plateau, this study focused on the Longyangxia to Liujiaxia region, a representative section of the UYR, which is significantly influenced by environmental controls and anthropogenic activities. This area encompasses both permafrost and seasonally frozen ground and regions that are characterized by the development of cascade reservoirs. Specifically, three deep reservoirs, namely, Longyangxia (LYX), Lijiaxia (LJX), and Liujiaxia (LJXX)[50,51]. Focusing on the scientific issues related to CO_2 and CH_4 emissions and their influencing mechanisms, the main objectives of this study were to (1) analyse the spatial and temporal distributions of the CO_2 and CH_4 concentrations and diffusive fluxes from three large reservoirs in the UYR, (2) elucidate the dominant processes governing CO_2 and CH_4 emissions under seasonal variations, (3) explore the key factors driving the CO_2 and CH_4 emissions from reservoirs of the plateau region, and reveal the complex environmental control mechanisms involved. The findings of this research provide a scientific basis for GHG emissions reduction and ecosystem management in the upper Yellow River Basin.

Materials and methods

Study area overview

The UYR (LYX to LJXX) is situated between 100°6'22"E to 103°26'16"E and 35°16'08"N to 36°17'20"N. This region spans the Qinghai and Gansu Provinces of China, covering a watershed area of approximately 9,499 km². The main stream extends approximately 355 km, with a natural elevation drop of approximately 838 m. The area features permafrost and seasonally frozen ground, as well as several major tributaries, including the Daxia River and the Tao River. The region experiences a typical continental alpine climate, which is characterized by low temperatures throughout the year, cool and rainy summers, and cold, dry winters. The temperatures gradually rise from northwest to southeast, with annual averages ranging from − 3 to 3 °C. Precipitation remains relatively stable during winter and spring, varying from 200 to 700 mm, and minimally fluctuates between adjacent years, with an annual average of approximately 520 mm[50,52].

This river section contains six large and medium-sized reservoirs. Among these, three reservoirs with the largest total capacities, listed from upstream to downstream, are Longyangxia (24.7 billion cubic meters), Lijiaxia (1.65 billion cubic meters), and Liujiaxia (5.72 billion cubic meters)[53,54]. The upper LYX Reservoir consist of pastoral areas, whereas the lower reaches are predominantly agricultural zones. Most irrigation water is sourced from branch ditches, with any shortfall supplemented by water from the Yellow River. Two major tributaries, the Daxia River and the Tao River, converge to the LJXX Reservoir, and the surrounding area is densely populated, leading to frequent human activities that may disrupt the natural hydrological rhythms, water temperatures, and other environmental factors of the main stream. Developments in agriculture and animal husbandry along LYX to LJXX remain limited and in a seminatural state, with no significant industrial pollution discharges occurring within the basin[35]. LYX to LJXX exemplifies a portion of the UYR that exhibits notable environmental specificity and sensitivity. It is characterized by the highest degree of cascade hydropower development and the most complete ecological pattern, which can, to some extent, reflect the environmental characteristics of the inland waters of the Tibetan Plateau. Consequently, greenhouse gas emissions from these reservoirs warrant significant attention.

Sample collection

In this study, the UYR (LYX to LJXX region) on the Tibetan Plateau was selected as the area of investigation. Surface water samples were collected during two distinct periods: January (the soil freezing period) and April (the soil thawing period) in 2024. These samples were collected from three large reservoirs, namely, LYX, LJX, and LJXX, which are distributed from upstream to downstream, as well as from part of the main stream. A total of 25 sampling sections were established throughout the LYX to LJXX region, consisting of 6 in the main stream and 19 in the tail, reservoir area, pre-dam, under-dam, and tributaries of the three reservoirs. The specific sampling locations are shown in Fig. 1 and Table S1.

Surface water samples were collected at a depth of 0.5 m below the water surface via a plexiglass water collector. These samples were stored in 500-mL high-density polyethylene containers that were shielded from light and maintained at low temperatures for subsequent water chemistry analyses. Aqueous samples for the determination of CO_2 and CH_4 were transferred using silicone tubing to sealed 20 mL glass serum bottles, and 0.5 mL of pre-configured saturated $HgCl_2$ solution (7.4% w/v, 25 °C) was injected into the serum vials to inhibit microbial activity, and the injection rate was controlled at 50 μL s^{-1} to avoid perturbation. Subsequently, serum vials were sealed with a rubber septum with a polytetrafluoroethylene liner and an aluminium cap, shaken well, and stored in the dark at low temperature. Each collection included two parallel samples.

In addition, we monitored the environmental conditions at the sampling sections via a multiparameter water quality meter (YSI EXO2, Gimcheon Instruments Inc., USA) to assess the water temperature (T_w), dissolved oxygen (DO), pH, oxidation-reduction potential (ORP), and electrical conductivity (EC) of the in situ water bodies. A portable alkalinity meter (Photometer 7500, Palintest, UK) was used to measure the alkalinity (Alk), whereas a portable multiparameter weather station (Model WXT520, Vaisala, Finland) was used to obtain air temperature (T_a) and wind speed data. The water flow velocities were determined using a galvanometer (Stalker II SVR, ACI, USA). The latitude, longitude, and altitude (Alti) of the sampling sections were recorded via GPS, and monthly mean precipitation (Precip) data were sourced from the China Meteorological Data Service Centre (http://data.cma.cn/). Observations of seasonally frozen ground were conducted in accordance with the Specifications for surface meteorological observation—General (https://www.cma.gov.cn/). Three-parameter soil sensors (Hydra Probe II, Stevens, USA) were installed in the area of seasonally frozen ground located upstream of LYX to LJXX (100°33'59"E and 36°7'48"N) region to encompass a complete freeze–thaw cycle during the sampling period. Daily observations of soil temperature (T_s) and water content (VWC) at depths of 10 cm, 20 cm, and 40 cm were recorded from 1 May 2023 to 30 April 2024 to elucidate the variations in the freeze–thaw cycles of the local seasonally frozen ground. The collection of water and soil samples used in this study was supported and facilitated by the Science and Technology Management Department and the local management of the study area. Meanwhile, water and soil samples were collected and processed in strict accordance with national environmental protection standards and relevant industry norms of China, including the Water quality—Guidance on sampling techniques (HJ 494-2009) and the Technical Specification for soil Environmental monitoring (HJ/T 166-2004). The sampling sites do not involve confidential or sensitive areas, and are open to the public, with no academic ethical disputes.

Sample analysis

The dissolved concentrations of CO_2 and CH_4 were determined via headspace equilibration[55]. After the samples were transported to the laboratory, the water in the serum vials was replaced with 10 mL of high-purity helium. The vials were then placed on a shaker for 1 min at room temperature with vigorous shaking. All the serum vials were subsequently inverted and left to stand overnight to allow the gases to equilibrate between the liquid and

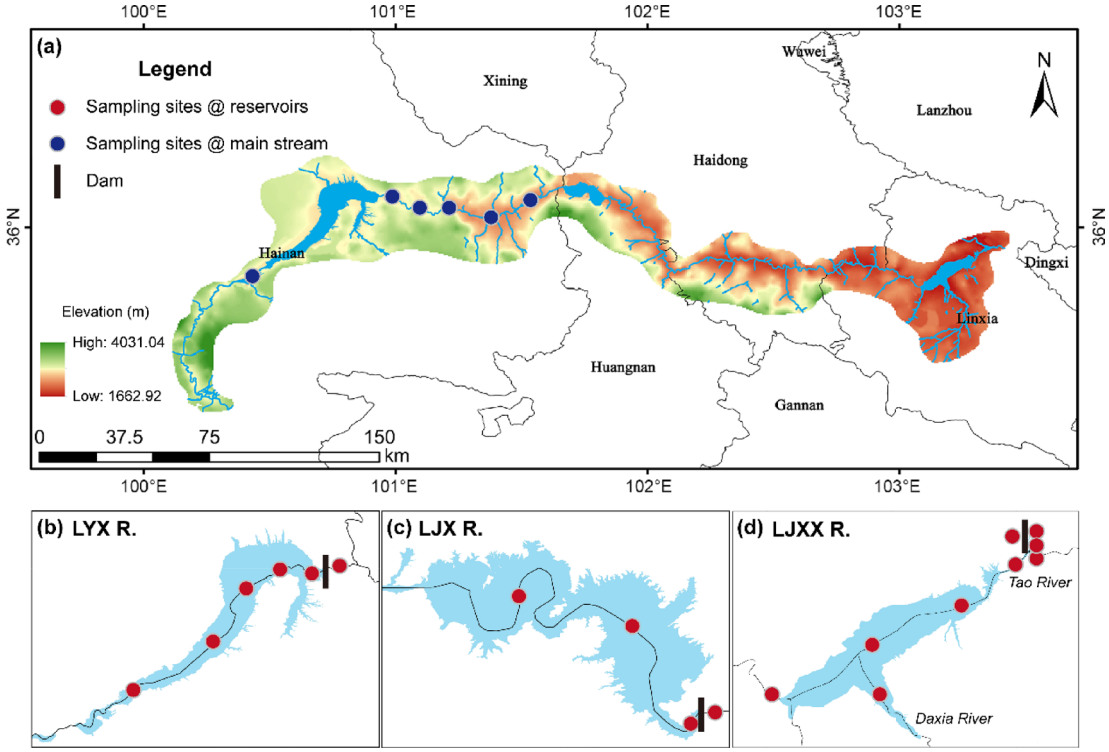

Fig. 1. The distribution of dams, catchment boundaries, and sampling sites in this study is illustrated as follows: (**a**) the upper Yellow River basin, (**b**) Longyangxia Reservoir, (**c**) Lijiaxia Reservoir, and (**d**) Liujiaxia Reservoir. The short black lines represent the dams, while the red circles indicate the sampling sites within the reservoirs, and the blue circles denote the sampling sites along the main stream. Detailed geographical information regarding the sampling sites is provided in the Supplementary Information (SI, Table S1). The map was created using ArcGIS Pro 3.1.2 (available at https://www.esri.com/en-us/arcgis/products/arcgis-pro/).

gas phases. A minimum of 3 mL of headspace gas was withdrawn via a syringe equipped with a three-way valve for injection into a three-valve, four-column Flame Ionization Detector (FID) + Thermal Conductivity Detector (TCD) dual-detector gas chromatograph (Agilent 7890 A, Agilent Co., USA) to determine the CO_2 and CH_4 concentrations. The calculation of in situ concentrations necessitated corrections for the distribution of gases in both the headspace and aqueous phases, as well as for their air pressures and volumes within the bottles, in accordance with Henry's law.

For the water chemistry analyses, water samples were examined to determine their dissolved organic carbon (DOC) and dissolved inorganic carbon (DIC) contents via an organic carbon analyser (Multi N/C 2100, Jena, Germany). Total nitrogen (TN) contents were determined through ultraviolet spectrophotometry, following the analytical procedure outlined by the National Standardization Administration (https://www.sac.gov.cn/), which utilized alkaline potassium persulfate as an oxidizing agent for digestion. The water samples were filtered through 0.45-μm cellulose acetate filter membranes (Whatman GF/F) to measure nitrate nitrogen (NO_3^--N) and ammonia nitrogen (NH_4^+-N) via UV spectrophotometry and nanoreagent spectrophotometry, respectively. Furthermore, the filtered membranes were stored frozen on dry ice and subsequently analysed using 90% acetone for extraction and determination of the chlorophyll-a (Chl-a) concentrations via spectrophotometry. The chemical oxygen demand (COD) was assessed via the potassium permanganate method.

Calculation of gas saturation and diffusion fluxes

Gas saturation

Gas saturation is determined by the ratio of the dissolved concentration of CO_2 (or CH_4) to the water–air equilibrium concentration. This ratio is calculated using the following Eqs[56].–[59]:

$$S_{gas} = \frac{C_{water}}{C_{eq}} \times 100\% \quad (1)$$

where S_{gas} is the gas saturation; C_{water} is the dissolved concentration of CO_2 (or CH_4) measured in μmol L^{-1}; and C_{eq} is the concentration of CO_2 (or CH_4) in water at the in situ water–air equilibrium, also expressed in μmol L^{-1}, which is typically derived by converting the saturated concentration of the gas in water at the same temperature and pressure as the in situ conditions to its concentration in air[58,59].

Furthermore, we analysed the relationship between ΔO_2 (the difference between the concentration of dissolved oxygen in water and its water–air equilibrium concentration) and ΔCO_2 (the difference between the concentration of dissolved CO_2 and its water–air equilibrium concentration) to elucidate the potential factors—

such as physical, chemical, and biological processes—that influence CO_2 and CH_4 production and release in aquatic ecosystems[60].

Diffusive fluxes of CO_2 and CH_4

The diffusive fluxes of CO_2 and CH_4 are estimated using model calculations based on the thin boundary layer (TBL) theory with the following basic formula[61]:

$$Flux = k \times (C_{water} - C_{eq}) \tag{2}$$

where *Flux* is the diffusive flux of CO_2 (or CH_4) at the water–air interface, measured in mmol m^{-2} d^{-1}. k is the gas exchange coefficient at the water–air interface expressed in cm h^{-1} and is calculated via the equation provided by Goldenfum[61].

$$k = k_{600} \times \left(\frac{S_c}{600}\right)^{-x} \tag{3}$$

where x is the adjustment factor, which is defined as 2/3 for wind speed (U_{10}) less than or equal to 3 m s^{-1} and 0.5 for a wind speed greater than 3 m s^{-1}. Here, U_{10} is the frictionless wind speed at 10 m expressed in m s^{-1}, which is calculated according to the equation provided by Goldenfum[61].

$$U_{10} = 1.22 \times U_1 \tag{4}$$

where U_1 is the wind speed at the water surface expressed in m s^{-1}.

S_c is the Schmidt number of CO_2 (or CH_4), unitless, and is calculated via the following Eq[61].:

$$S_c\,(CO_2) = 1911.1 - 118.11 \times t + 3.4527 \times t^2 - 0.04132 \times t^3 \tag{5}$$

$$S_c\,(CH_4) = 1897.8 - 114.28 \times t + 3.2902 \times t^2 - 0.039061 \times t^3 \tag{6}$$

where t is the water temperature in degrees Celsius (°C).

k_{600} is the gas exchange coefficient expressed in cm h^{-1} normalised for CO_2 at 20 °C in fresh water with a Schmidt number of 600. The calculation of k_{600} varies on the basis of the type of water and the mixing conditions at the water–air interface[35]. In this study, k_{600} is calculated using the following equation:

$$k_{600} = 2.07 + 0.215 \times {U_{10}}^{1.7} \tag{7}$$

$$k_{600} = 0.45 \times {U_{10}}^{1.64} \tag{8}$$

$$k_{600} = 2.02 + VS \times 2841 \tag{9}$$

where V is the water flow velocity expressed in m s^{-1} and S represents the slope of the river, which is unitless. Equations (7) and (8) are relevant for reservoir water bodies[35,61]. Specifically, Eq. (7) is utilized when U_{10} is less than or equal to 3 m s^{-1}, whereas Eq. (8) is applied when U_{10} exceeds 3 m s^{-1}. Equation (9) is applicable to river water bodies[56,62]with a particular emphasis on calculating GHG emissions in rivers located on the Tibetan Plateau[63].

The total CO_2 and CH_4 emissions from the three reservoirs, along with those from the entire river section, are assessed in terms of the CO_2 equivalent (CO_2-eq) values to express the global warming potential (GWP). Specifically, the GWP of CH_4 is 34 times greater than that of CO_2 over a 100-year horizon[56,64].

Statistical analysis

In this study, environmental factors were classified into three categories of sources of influence: physicochemical properties (e.g., T_w, DO, pH, ORP, EC, Alk and COD); productivity (e.g., TN, NH_4^+-N, NO_3^--N, DOC, DIC and Chl-a); and natural geography (e.g., Precip, T_a and Alti). Prior to conducting the statistical analyses, all the measured variables were subjected to normal distribution tests and variance homogeneity tests via the Shapiro–Wilk tests and F tests, respectively. Log-transformations were applied to some variables to satisfy the normality assumption; however, it did not fulfil the heteroscedasticity assumption. Consequently, Welch's ANOVA test was employed for two comparisons, and Tamhane's T2 test was utilized for multiple comparisons to analyse the significant differences among seasons and reservoirs concerning environmental factors, as well as the CO_2 and CH_4 dissolved concentrations and diffusive fluxes. Correlations between the CO_2 and CH_4 concentrations and environmental factors were analysed using Pearson's correlations and linear regressions in IBM SPSS Statistics Version 17.0 to identify the predictors. To avoid the effects of multicollinearity on the model results, stepwise multiple linear regression (MLR) was employed to reduce the number of predictors and identify the key explanatory variables[65]. Redundancy analysis (RDA) was conducted using CANOCO Version 5.0 to assess the relative influences of different environmental factors on the dissolved CO_2 and CH_4 concentrations and diffusive fluxes. Partial least square structural equation modelling (PLS-SEM) was performed in R Version 4.1.0 via the 'semPLS' package to quantify the direct and indirect effects of environmental factors on the CO_2 and CH_4 emissions. The model fit was evaluated as good on the basis of the following criteria: $\chi^2/df < 3$; RMSEA < 0.1; and GFI, CFI, and NFI > 0.9. The significance level for all tests was set at $p < 0.05$, and the statistical results are expressed as the means ± standard errors.

Results

Soil freeze–thaw seasonal evolution processes

Climate changes, including variations in temperature and precipitation, directly or indirectly influence the dynamic balance of carbon in the active layer of frozen ground. This results in the release of carbon from the soil into the atmosphere, as well as the lateral input of carbon into surrounding water bodies. To investigate the seasonal variations in the CO_2 and CH_4 emissions from surface water in the UYR (LYX to LJXX), we analysed the freeze–thaw processes of local seasonally frozen ground during the sampling period. This analysis aimed to define the time scales of different soil freeze–thaw periods accurately (Fig. 2). Among the key factors affecting soil carbon emissions are the soil freezing temperature and water content[66,67]. Consequently, this study first delineated the freezing and thawing periods of frozen ground by examining the characteristics of the interannual variations of these two critical variables, namely, soil temperature and water content, at various depths. Second, we tested the significance of the differences between the defined freezing and thawing periods to ensure the reliability and representativeness of the selected time scales.

At the beginning of December, the temperatures of the top and middle soil layers (10 cm and 20 cm, respectively) fell below 0 °C, approaching the freezing point. This led to the onset of soil freezing and a significant decrease in the soil water content. The soil temperatures subsequently continued to decrease under the influence of atmospheric conditions, reaching their minimum values at the end of January. Excluding the effects of short-term weather extremes, the surface soil temperatures decreased to approximately -6 °C, whereas the water contents stabilized at minimum values of 0.05 m^3 m^{-3}. In early March, the surface and intermediate soil temperatures gradually rose above 0 °C, initiating the thawing process and resulting in an increase in water content. From early March until the end of June, the surface soil temperatures continued to recover, peaking at approximately 26 °C at the beginning of July, at which point all the frozen ground had melted. During this thawing period, the soil water content fluctuated steadily at 0.2 m^3 m^{-3}. From early July to the end of October, the soil temperature gradually decreased, and by mid-November, the temperature of the subsoil (40 cm) was the first to drop below 0 °C, while the surface and middle soil temperatures hovered around 0 °C, indicating the beginning of frozen ground formation. On the basis of the regular analysis of the freeze–thaw processes mentioned above, the period from early November to the end of February was designated the freezing period. Specifically, November and December were identified as the frozen ground development stage, whereas January and February represented the stabilization stage or freezing bloom. The period from early March to the end of June was classified as the thawing period, with March and April experiencing the most intense thawing activity. The sampling times were January and April, which corresponded to the freezing bloom and early thawing stages,

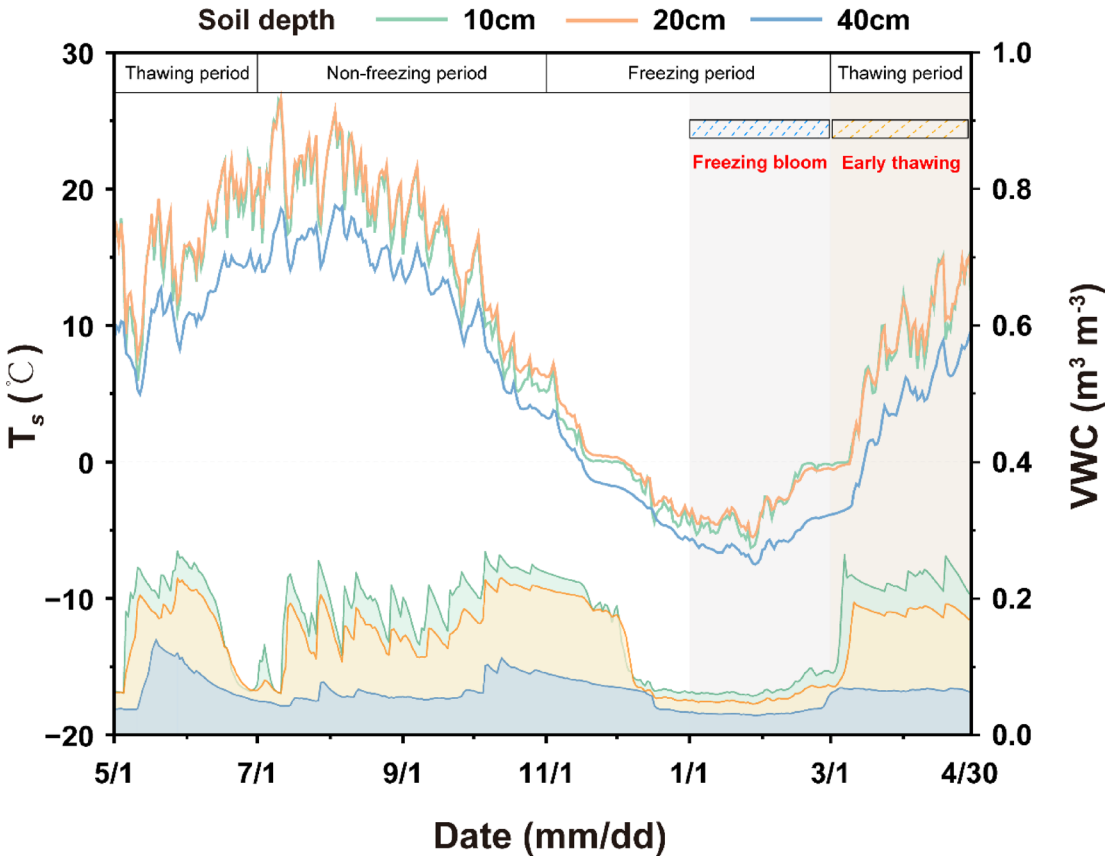

Fig. 2. Soil temperature (T_s) and soil water content (VWC) change vary over time at different depths, delineating the freeze–thaw stage (freezing period [FP] and thawing period [TP]) and non-freeze–thaw stage.

respectively, and were representative of the freezing and thawing periods. Consequently, January and February were defined as the freezing period (FP), and March and April were designated the thawing period (TP) for this study. Notably, highly significant differences in soil temperature and water content at all depths were observed between the freezing and thawing periods ($p < 0.001$, Fig. 3).

Spatial and temporal variations in CO_2 and CH_4 concentrations and fluxes

The range of CO_2 dissolved concentrations (C_{CO2}) at each sampling site in the UYR (LYX to LJXX) varied between 89.34 and 219.21 μmol L^{-1}. The mean C_{CO2} value was calculated to be 132.59 ± 30.31 μmol L^{-1}, which was 5.66 times greater than the mean value of atmospheric equilibrium (see Table S2). These findings indicated that C_{CO2} was supersaturated in all surface waters throughout the study period. Additionally, C_{CO2} exhibited significant seasonal variations, with levels notably greater during the TP (146.17 ± 34.57 μmol L^{-1}) than during the FP (117.16 ± 13.30 μmol L^{-1}) ($p < 0.05$; Table S2). The overall variations in the dissolved CH_4 concentrations (C_{CH4}) were substantial, ranging from 3.24 to 674.71 μmol L^{-1} (S_{CH4} from 0.4×10^5 to 108×10^5), with a mean value of 60.68 ± 104.80 μmol L^{-1} (S_{CH4} of $8.86 \times 10^5 \pm 16.56 \times 10^5$). The water bodies from LYX to LJXX were strongly supersaturated with C_{CH4}, acting as a net source of CH_4 emissions. Furthermore, the C_{CH4} levels were significantly greater during the TP (86.40 ± 139.60 μmol L^{-1}) than during the FP (31.46 ± 10.26 μmol L^{-1}) ($p < 0.05$, Table S2). C_{CO2} and C_{CH4} exhibited distinct spatial variations across different freeze-thaw periods throughout the UYR (LYX to LJXX) (Fig. 4 and Fig. S1). During the FP, both C_{CO2} and C_{CH4} tended to stabilize in the water bodies from LYX to LJXX, which was attributed to lower air and water temperatures as well as reduced primary production. In contrast, during the TP, the C_{CO2} levels were higher in the LYX reservoir than other reservoirs. The C_{CH4} levels were highest in the LJXX reservoir. Owing to significant sediment siltation upstream of the dam at the LJXX Reservoir and the intensification of human activities, the C_{CH4} levels in the primary tributary, the Tao River, reached 674.71 μmol L^{-1}, surpassing those of the two upstream reservoirs and establishing it as a hotspot for CH_4 emissions following the confluence with the Tao River.

In this study, the k_{600} values utilized for the gas flux calculations ranged from 2.32 to 27.25 cm h^{-1}. The CO_2 diffusive fluxes (F_{CO2}) that were obtained for each sampling site, on the basis of the C_{CO2} and k_{600} calculations, ranged from 31.50 to 505.27 mmol m^{-2} d^{-1}, with an overall mean of 190.34 ± 102.78 mmol m^{-2} d^{-1}. Notably, the F_{CO2} values during the TP (239.32 ± 94.43 mmol m^{-2} d^{-1}) were significantly greater than those during the FP (134.69 ± 82.76 mmol m^{-2} d^{-1}) ($p < 0.05$, Table S2). The highest F_{CO2} value was observed in the high-elevation, nutrient-poor LYX Reservoir, which presented a flux of 253.20 ± 93.97 mmol m^{-2} d^{-1}. The range of CH_4 diffusive fluxes (F_{CH4}) was 6.35 to 1765.32 mmol m^{-2} d^{-1}, with a mean value of 128.87 mmol m^{-2} d^{-1}. Similarly, the F_{CH4} values were significantly greater during the TP (201.12 ± 366.57 mmol m^{-2} d^{-1}) than during the FP (46.77 ± 33.56 mmol m^{-2} d^{-1}) ($p < 0.05$, Table S2). The maximum F_{CH4} concentration was recorded in the LJXX Reservoir, which presented a relatively high downstream sediment load (261.62 ± 480.48 mmol m^{-2} d^{-1}). Overall, the total CO_2 and CH_4 emissions across the entire river section indicated that the carbon emissions during the TP were 4.1 times higher than those during the FP. Furthermore, the LJXX Reservoir emerged as a hotspot for GHG emissions, with a release flux of 9.06 ± 16.41 mol CO_2-eq m^{-2} d^{-1}, which was 3.3 times greater than that of the LYX Reservoir and 5.8 times greater than that of the LJX Reservoir during the same period.

CO_2 and CH_4 concentrations and fluxes in relation to environmental factors

Pearson's correlations of all the environmental factors revealed significant and positive correlations of C_{CO2} with Precip, Alti, T_a, and COD, whereas C_{CO2} was significantly negatively correlated with pH, Chl-a, and DO ($p < 0.05$, Fig. 5a). Unary linear regressions indicated that DO, Precip, COD, and Alti were potential predictors of surface water C_{CO2} values from LYX to LJXX; however, the explanatory power of these predictors was relatively weak, with linear regression coefficients (R^2 of 0.230, 0.216, 0.207, and 0.191, respectively (Fig. 6). In contrast, Chl-a, pH, and T_a accounted for 13.5%, 12.4%, and 11.4% of the variances in C_{CO2}, respectively (Fig. 6). Furthermore,

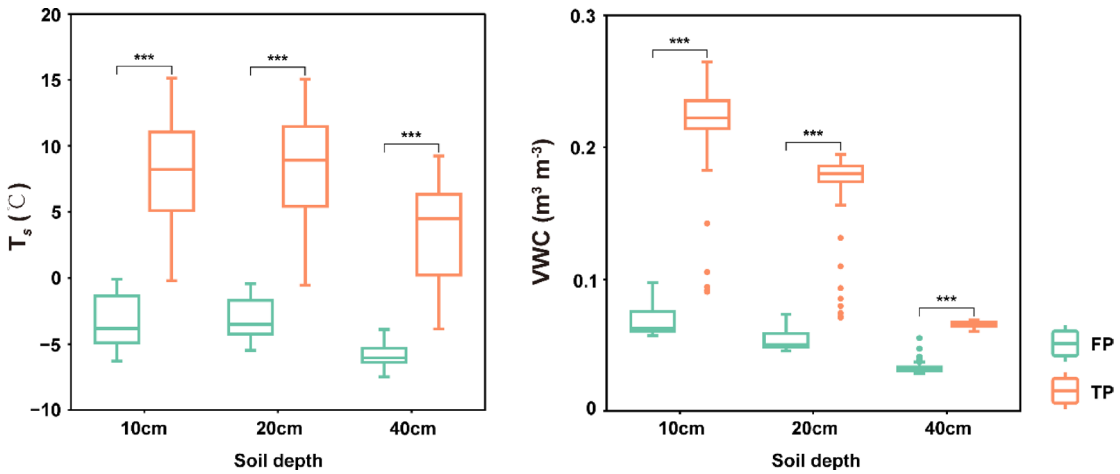

Fig. 3. Box plots of T_s and VWC at different depths during the FP and TP are presented. The significance level of correlations is indicated with ***$p < 0.001$.

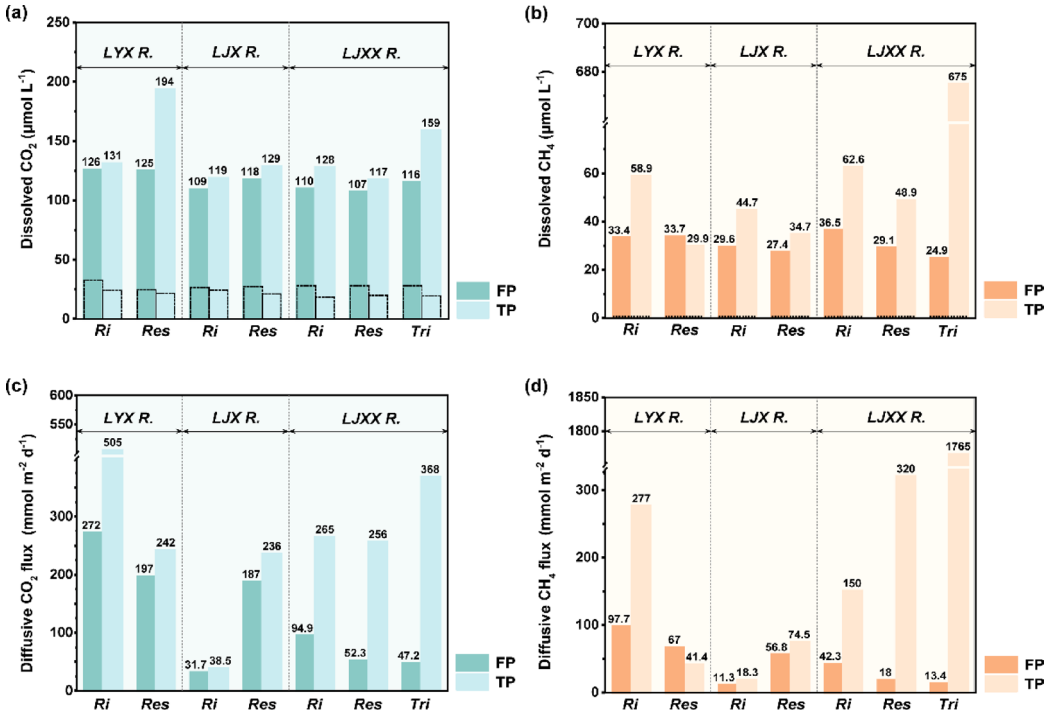

Fig. 4. The spatial variability of (**a**) dissolved CO_2 concentration [C_{CO2}], (**b**) dissolved CH_4 concentration [C_{CH4}], (**c**) diffusive CO_2 flux [F_{CO2}], and (**d**) diffusive CH_4 flux [F_{CH4}] in water bodies in the upper Yellow River (UYR) from three large reservoirs (LYX, LJX and LJXX). FP represents the soil freezing period, TP represents the soil thawing period, and the dashed boxes represent the atmospheric equilibrium concentrations of CO_2 or CH_4.

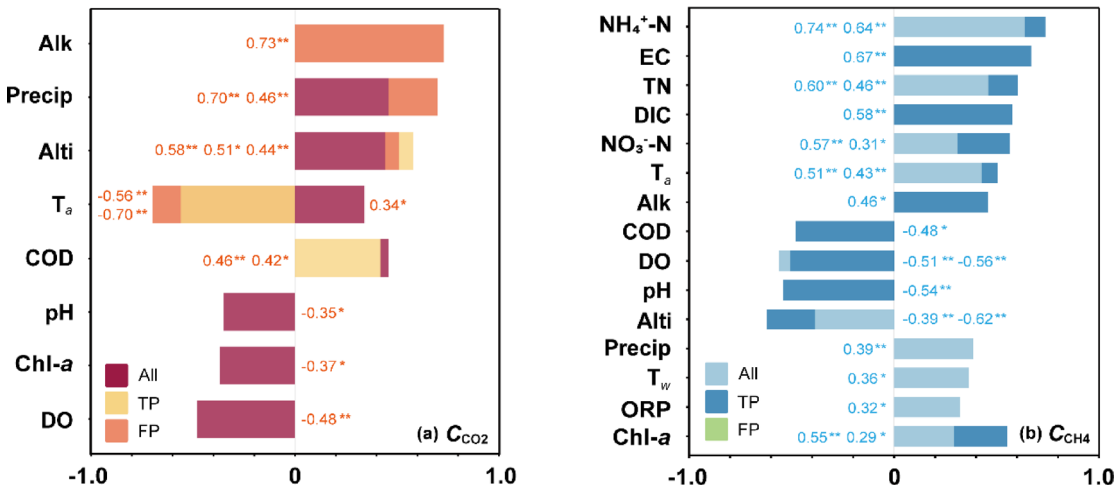

Fig. 5. The Pearson's correlations between (**a**) C_{CO2}, (**b**) C_{CH4} and key environmental factors in surface water in the UYR (LYX to LJXX). The significance levels of the correlations are indicated as $^*p<0.05$ and $^{**}p<0.01$, respectively.

MLR indicated that C_{CO2} could be jointly explained by DO and Alti, yielding an explanatory power of 38.3% ($p<0.001$, Fig. 7 and Table S3). Notably, there was no significant relationship between the C_{CO2} and nutrient concentrations, including TN, NH_4^+-N, NO_3^--N, DOC, and DIC (Fig. S2), suggesting that the variations in carbon and nitrogen from LYX to LJXX had a limited effect on C_{CO2}. Additionally, when the relationships between C_{CO2} and environmental factors during the soil freezing and thawing periods were examined, Alk was found to be highly positively correlated with C_{CO2} during the FP, explaining 44.2% of the variation in C_{CO2} ($p<0.001$, Fig. 5a and Fig. 6), whereas this correlation was not significant during the TP. T_a exhibited significant

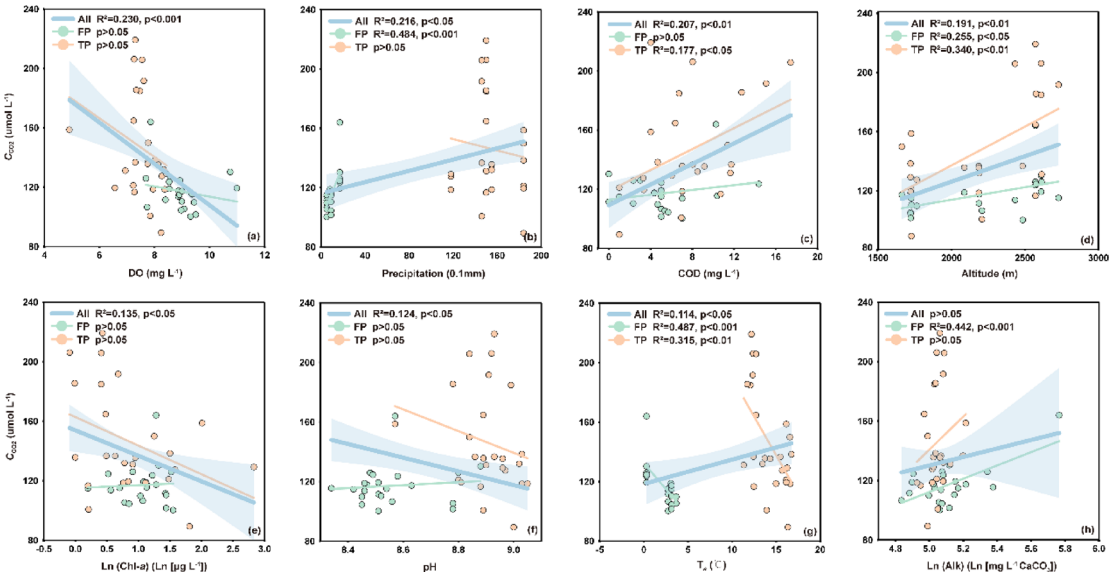

Fig. 6. The relationship between C_{CO2} and (**a**) dissolved oxygen [DO], (**b**) Precipitation, (**c**) chemical oxygen demand [COD], (**d**) Altitude, (**e**) Ln(chlorophyll-a) Ln[Chl-a], (**f**) pH, (**g**) air temperature [T_a], and (**h**) Ln(alkalinity) Ln[Alk] in surface water in the UYR (LYX to LJXX).

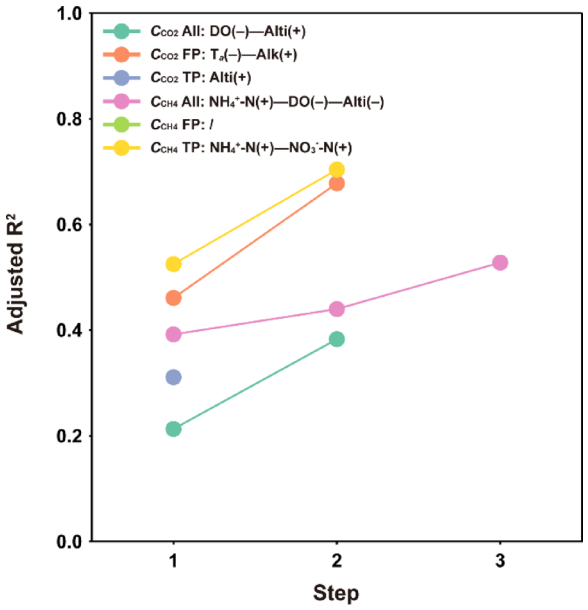

Fig. 7. Multiple stepwise regression analysis (MLR) is conducted with C_{CO2} and C_{CH4} as dependent variables and environmental factors as independent variables, in surface water in the UYR (LYX to LJXX) during different periods. The final set of model predictors for each regression is presented in sequence, ordered by their relative importance in explaining the dependent variables. Note that "+" and "–" in brackets indicate positive and negative relationships, respectively, between C_{CO2}, C_{CH4} and the predictors.

negative correlations with C_{CO2} in both periods ($p < 0.01$, Fig. 5a), despite showing a positive correlation in the overall analysis.

To further illustrate the interrelationships between C_{CO2} and F_{CO2}, along with their associations with environmental variables across LYX to LJXX and the seasonal variations, all the data were analysed using RDA and PLS-PM. The RDA results indicated that the two principal components (RDA1 and RDA2) accounted for 52.1% and 15.7% of the variance in the variables, respectively (Fig. 8a). The variables, T_w, DO, pH, Precip, and T_a, were highly correlated with RDA1, which encompasses physicochemical and natural geographical factors. DOC, NH_4^+-N, and Chl-a were associated with RDA2, representing the productivity factors. During the two distinct freeze–thaw periods, the data points exhibited significant divergence, with C_{CO2} and F_{CO2} serving as the

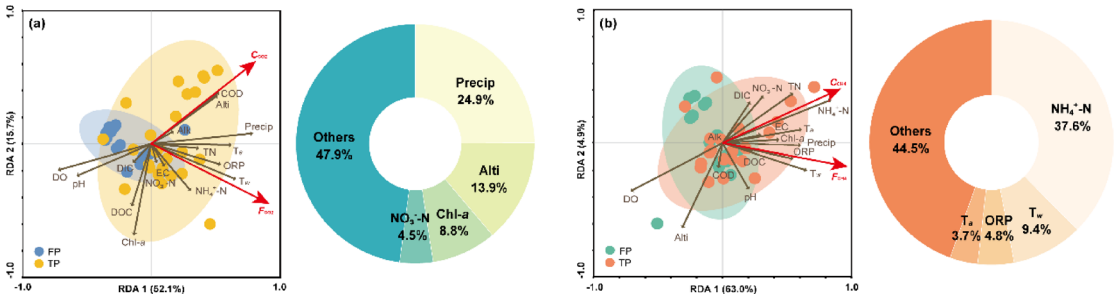

Fig. 8. The results of the redundancy analysis (RDA) for (a) CO_2 emissions [C_{CO2} and F_{CO2}] and (**b**) CH_4 emissions [C_{CH4} and F_{CH4}] are presented, showing the loadings associated with different environmental factors. The pie charts illustrate the percentages of variance in CO_2 and CH_4 emissions that are explained by these different variables.

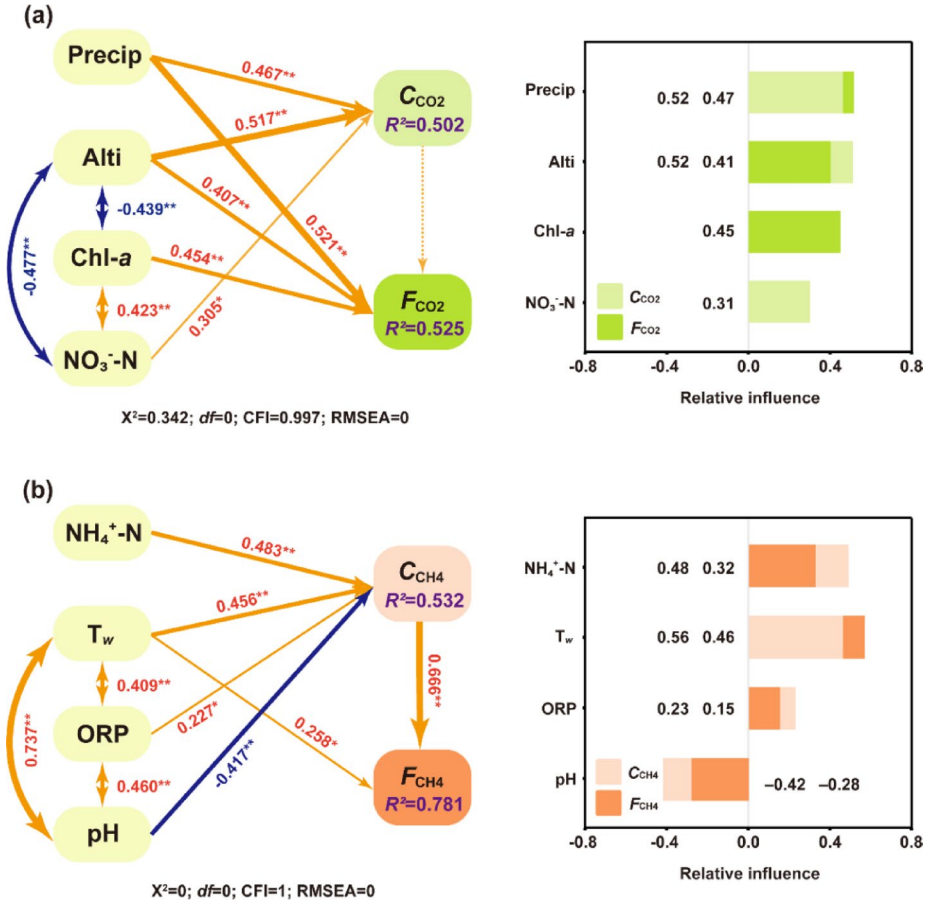

Fig. 9. Partial least squares structural equation modelling (PLS-SEM) is employed to evaluate the direct and indirect effects of environmental factors on (**a**) C_{CO2} and F_{CO2}, and (**b**) C_{CH4} and F_{CH4}. Solid blue and orange arrows indicate significant positive and negative effects, respectively, while dotted arrows represent insignificant effects on the dependent variable. The numbers adjacent to the arrows denote standardized path coefficients, which indicate the effect size of the relationships. The R^2 value represents the variance explained for the target variables. The significance levels of the correlations are indicated as $^*p < 0.05$ and $^{**}p < 0.01$, respectively.

principal components that were correlated with RDA1 and RDA2, respectively. The seasonal variations in C_{CO2} and F_{CO2} were influenced by Precip, Alti, Chl-a, and NO_3^--N, collectively accounting for 52.1% of the variations (Fig. 8a). According to the PLS-PM, Precip and Alti had direct positive effects on both C_{CO2} and F_{CO2}, whereas NO_3^--N and Chl-a positively influenced C_{CO2} and F_{CO2}, respectively. Additionally, Chl-a and NO_3^--N positively affected one another, whereas Alti had negative effects on both Chl-a and NO_3^--N (Fig. 9a).

The correlations between C_{CH4} and various environmental factors are illustrated in Fig. 5b. C_{CH4} was significantly positively correlated with TN, NH_4^+-N, NO_3^--N, T_a, T_w, ORP, Chl-a, and Precip ($p < 0.05$) but was significantly negatively correlated with DO and Alti ($p < 0.01$, Fig. 5b). Upon analysing all the measurements, NH_4^+-N emerged as a stronger predictor of C_{CH4} in surface water from LYX to LJXX, accounting for 40.5% of the variance in C_{CH4} (Fig. 10). In contrast, DO and TN, identified as relatively weak predictors, explained 31.6% and 22.8% of the total F_{CH4} variance, respectively (Fig. 10). Although the correlation analysis yielded statistically significant results ($p < 0.05$), many environmental factors, including T_a, T_w, Precip, Alti, ORP, NO_3^--N, and Chl-a, only weakly explained the variability in F_{CH4} ($R^2 < 0.200$, Fig. 10). Furthermore, variations in the explanatory powers and predictors of C_{CH4} were observed during the freeze–thaw stage. During the FP, no key predictors of C_{CH4} were identified; however, during the TP, NH_4^+-N and NO_3^--N collectively accounted for 70.4% of the total C_{CH4} variability (Fig. 7 and Table S3), underscoring the importance of the biogenic substance, nitrogen, for C_{CH4}.

The RDA and PLS-PM of C_{CH4} and F_{CH4}, which consider all the environmental factors, revealed that RDA1 and RDA2 accounted for 63.0% and 4.9% of the variances in the variables, respectively (Fig. 8b). C_{CH4} and F_{CH4} were strongly correlated with RDA1, which included NH_4^+-N, T_w, ORP, and T_a, collectively explaining 55.5% of the variance (Fig. 8b). C_{CH4} was positively influenced by NH_4^+-N, T_w, and ORP but was negatively affected by pH. These relationships subsequently influenced F_{CH4}, with T_w also having a direct positive effect on F_{CH4}. The direct and indirect effects of these variables largely accounted for the variance observed in F_{CH4} ($R^2 = 0.781$, Fig. 9b). Furthermore, T_w and ORP, ORP and pH, as well as T_w and pH, exhibited positive interrelationships (Fig. 9b).

Discussion

Dominant processes of CO_2 and CH_4 emissions under seasonal variations

Based on the "Paired O_2-CO_2 Measurements Framework" proposed by Vachon et al. (2020)[60]the differences in the $\Delta O_2/\Delta CO_2$ relationship between the freezing and thawing periods of reservoir water bodies can be analysed, which can reveal the dominant controlling mechanism of the CO_2 and CH_4 emissions at different freeze-thaw stages. In terms of atmospheric equilibrium, aerobic aquatic systems typically follow the theoretical line of $\Delta O_2/\Delta CO_2 \approx 1{:}{-1}$ (corresponding to the stoichiometric ratio of glucose metabolism), and deviations from this line are indicative of synergistic interactions of biological, chemical and physical processes[60,68,69].

The three deep reservoirs in the study area did not experience ice closure throughout the year, although they located in high alpine and high altitude areas. Intense solar radiation may be a key factor influencing the biogeochemical processes inside the reservoirs. $\Delta O_2/\Delta CO_2$ offset analyses showed that photochemical degradation of organic carbon during freezing period consumed more O_2 relative to the production of CO_2 (mean value of the offset: -14.31 ± 24.4, Fig. 11a and b), which is consistent with the dominant process of CO_2 release from photochemical oxidation of DOC in Arctic freshwater environments, which has similarities between the two aqueous environments[70]. In contrast, microbial-mediated anaerobic processes during the thawing period consume less O_2 relative to CO_2 production (mean value of offset: 6.66 ± 27.68, Fig. 11a and b). Notably, the offset was significantly and negatively correlated with CH_4 concentration ($R^2 = 0.164$, $p < 0.05$, Fig. 11c), possibly indicating that at least part of the pathway in anaerobic processes is related to the CH_4 production process in sediments[71]. It is worth noting that both water photo-oxidation and anaerobic metabolism processes are affected by the level of trophic state of the reservoir, leading to the limitation of this qualitative conclusion, which needs

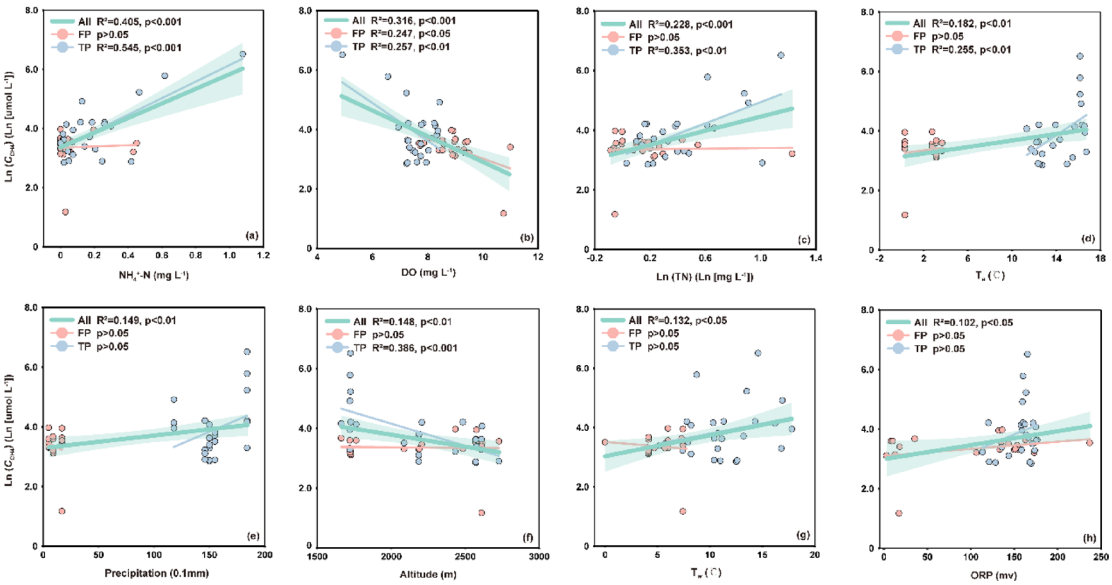

Fig. 10. The relationship between Ln(C_{CH4}) and (**a**) ammonia nitrogen [NH_4^+-N], (**b**) DO, (**c**) Ln(total nitrogen) Ln[TN], (**d**) T_a, (**e**) Precipitation, (**f**) Altitude, (**g**) water temperature [T_w], and (**h**) oxidation-reduction potential [ORP] in surface water in the UYR (LYX to LJXX).

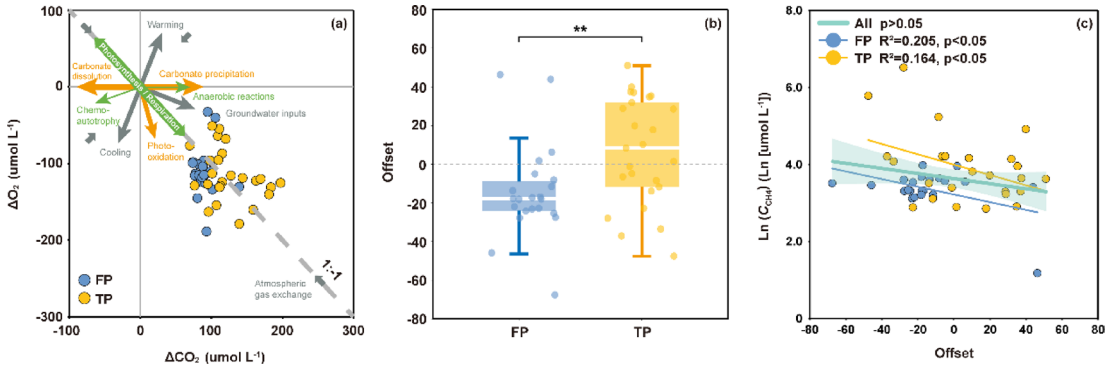

Fig. 11. (**a**) The relationship between the O_2 departure from atmospheric equilibrium (ΔO_2) and excess CO_2 (ΔCO_2) in surface water in the UYR (LYX to LJXX) during the FP and TP is illustrated. Arrows indicate the potential role of the different drivers[60]. (**b**) Box plots depict the offset (distance to the 1:−1 line, with values above the 1:−1 line labelled as positive and those below as negative) during the FP and TP. The significance level of correlations is indicated with $^{**}p < 0.01$. (**c**) The relationship between the offset and log-transformed C_{CH4} is presented.

to be analysed quantitatively in combination with the photosynthetic quotient (PQ) and the respiratory quotient (RQ) in the future.

In conclusion, CO_2 and CH_4 emission processes from reservoirs during different freeze-thaw stages are driven by two different metabolic mechanisms. During the freezing period, organic carbon releases CO_2 mainly through photochemical oxidation, whereas during the thawing period, microbial anaerobic metabolism becomes the main pathway for CH_4 generation, accompanied by photochemical degradation processes.

Main controlling factors of CO_2 and CH_4 emissions and their driving processes

Effects of physicochemical factors on CO_2 and CH_4 emissions

(1) CO_2 emissions

CO_2 dynamics in reservoirs are synergistically regulated by biological metabolism and carbonate balance (Fig. 12)[5]. Dissolved oxygen (DO) and chemical oxygen demand (COD) are direct and indirect indicators of water body biological metabolism, while pH and alkalinity (Alk) are important factors characterising the carbonate balance of the water body. Significant negative correlation between CO_2 and DO ($R^2 = 0.230$, $p < 0.001$) confirmed the contribution of heterotrophic respiration to CO_2 emissions, which is consistent with the findings of recent studies on lakes of the Tibetan Plateau[72]. High COD inputs significantly drive CO_2 emissions from the reservoirs. Downstream of the gradient reach (LJXX Reservoir), slowing water flow and sewage inflow from tributaries of the Daxia and Tao Rivers resulted in the accumulation of readily degradable organic matter, accelerating mineralisation and releasing CO_2[73,74]. CO_2 was significantly and positively correlated with COD ($p < 0.01$), Liu et al. (2023)[75] and Wang et al. (2023)[76] have observed similar mechanisms in inland waters in China. In addition, enhanced human activities during the thawing period resulted in significantly higher COD concentrations than during the freezing period ($p < 0.05$, Table S4), suggesting that the amplification effect of COD on CO_2 in alpine reservoirs is more pronounced during the thawing period, reflecting the coupling process between human activities and hydrological processes in the cryosphere region. The high pH (> 8.0) and high alkalinity (Alk) of the upper Yellow River waters significantly suppressed CO_2 emissions through carbonate chemical equilibrium[26,77]. The negative correlation of CO_2 with pH ($p < 0.05$) and positive correlation with Alk ($R^2 = 0.460$, $p < 0.05$ during the freezing period) found in this study corroborates the central role of the carbonate system.

(2) CH_4 emissions

Dissolved oxygen (DO) and pH are key constraints in the water column that affect CH_4 emissions. For DO, anaerobic decomposition processes in the water column are important to maintain high CH_4 production and release[35,78,79]. This is consistent with the significant negative correlation between CH_4 and DO in this study ($p < 0.01$). CH_4 emission may be influenced by the co-regulation of water column and sediment pH. In alkaline water environments, CH_4 can be released by chemical oxidation to CO_2 during transport along the water column to the upper layers. Results from a typical salt lake ecosystem showed that the oxidation efficiency of CH_4 in alkaline waters reached 91%, effectively reducing the atmospheric emission flux of CH_4[80]. In addition, high sediment pH has an inhibitory effect on the community dominance and metabolic functions of methanogenic bacteria[35,81]. Specifically, methanogenic bacteria were dominant at sediment pH < 7.5[82], whereas the activity of key enzymes for CH_4 production was significantly reduced at pH > 8[83]. In the present study, the mean pH values of the vertical water column and sediments of the reservoir were 8.74 and 8.39, respectively, during the study period, with an overall alkaline environment (Table S4 and Fig. S4), and this alkaline condition may have inhibited the metabolic activities of methanogenic bacteria, while facilitating the process of conversion of CH_4 to CO_2, thus reducing the emission of CH_4 to the atmosphere. Correlation analysis and PLS-SEM results showed that CH_4 concentration during the thawing period was significantly negatively correlated with pH ($R^2 = 0.292$,

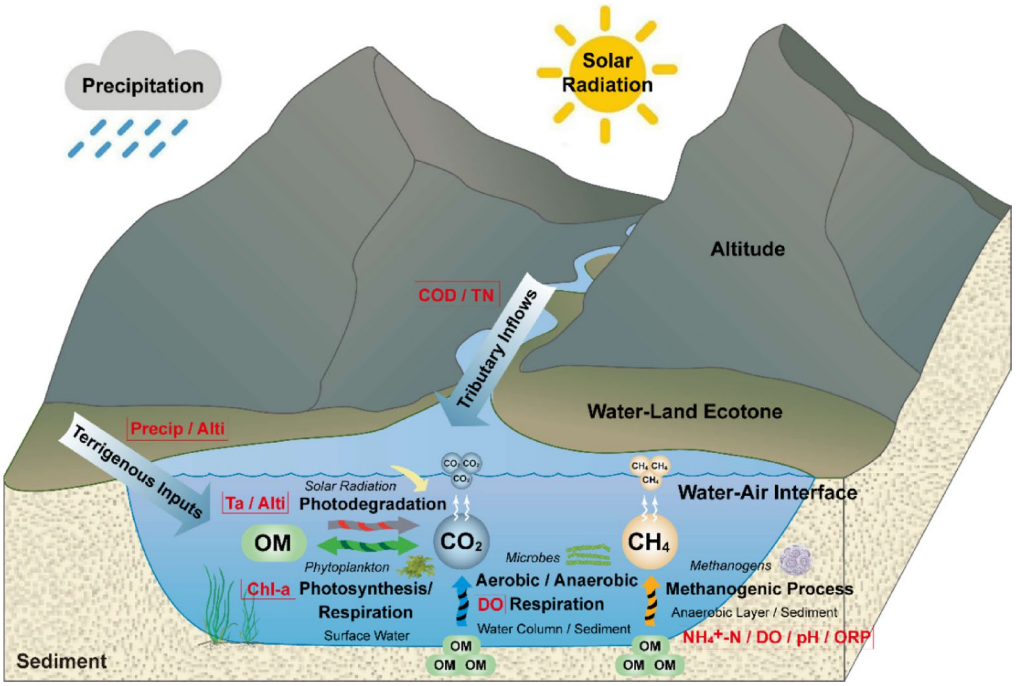

Fig. 12. Schematic depicting the main controlling factors of CO_2 and CH_4 emissions and their driving processes from reservoirs in the plateau region in this study. The primary driving processes include photodegradation, photosynthesis, aerobic and anaerobic respiration, methanogenic, terrigenous inputs and tributary inflows. The main controlling factors are T_a, Alti, Chl-a, DO, NH_4^+-N, pH, ORP, Precip, COD and TN. The figure was created using Adobe Illustrator 2024 (available at https://www.adobe.com/products/illustrator.html).

$p < 0.01$), and that pH had a significant negative regulatory effect on CH_4 production ($p < 0.01$, Fig. 9b), which further confirmed the possibility of the above mechanism.

Effects of productivity factors on CO_2 and CH_4 emissions

(1) CO_2 emissions

The relationship between chlorophyll a (Chl-a) and dissolved organic carbon (DOC), a key indicator of carbon metabolism processes in aquatic systems, and CO_2 concentration can reflect the relative contributions of photosynthetic carbon fixation and heterotrophic respiration to CO_2 fluxes. In natural river systems, oxidative decomposition of organic carbon dominates CO_2 emissions, leading to a generally significant positive correlation between CO_2 concentrations and DOC[26,84–87]. However, the LYX to LJXX in this study area has unique habitat characteristics due to the construction of the cascade reservoir complex, and the extension of hydraulic retention time in the reservoir area led to a significant increase in the plankton biomass, so that CO_2 produced by heterotrophic respiration of DOC as a substrate was offset by autotrophic production. At the same time, the low vegetation cover in the watershed and the poor soil organic carbon content resulted in lower exogenous DOC input fluxes compared to natural rivers[77]. Therefore, no significant correlation between CO_2 concentration and DOC was identified in this study, but a significant negative correlation was found between CO_2 concentration and Chl-a ($p < 0.05$, Fig. 5a), suggesting that by reshaping the metabolic balance of the water body, the cascade reservoirs have shifted the emission of CO_2 from traditional heterotrophic dominance to autotrophic regulation[68,88–90].

(2) CH_4 emissions

Productivity factors usually act as the main drivers of CH_4 emissions in reservoirs[22,23]and Chl-a may be associated with CH_4 producing related organic carbon enrichment[64,91,92].The positive correlation ($p < 0.05$) between CH_4 and Chl-a suggests that the prolonged hydrodynamic retention time in reservoirs allows for the vigorous growth of primary producers, such as algae, which not only leads to the formation of anaerobic zones, but also their growth metabolism and dead residues provide a large amount of organic matter for the emission of CH_4[37,93,95], a phenomenon that was more pronounced during the thawing period when microbial activity was higher ($R^2 = 0.306$, $p < 0.01$).

Nutrient may be involved in the in situ CH_4 production process by providing substrate and inhibiting oxidation. In anaerobic environments, methanogenic bacteria convert organic matter to CH_4 through metabolic activities, and nutrient provide the necessary substrate for this process, thus facilitating CH_4 production[96]. In addition, ammonium nitrogen (NH_4^+-N) has an inhibitory effect on methane-oxidising bacteria, effectively blocking further oxidation of the generated CH_4[97]. Therefore, higher nutrient concentrations generally favour CH_4 production and emission[36,98]. The results of this study showed that CH_4 concentration was significantly

and positively correlated with total nitrogen (TN), NH_4^+-N and nitrate nitrogen (NO_3^--N) ($p<0.05$), with NH_4^+-N proving to be a valid predictor of CH_4 emissions ($R^2=0.405$, $p<0.001$). During the thawing period with strong microbial metabolic activity, NH_4^+-N and NO_3^--N were able to explain most of the changes in CH_4 concentrations, suggesting that NH_4^+-N plays a key regulatory role in the production and release of CH_4, and is an important limiting factor in the process of its generation.

Effects of natural geographic factors on CO_2 and CH_4 emissions

(1) CO_2 emissions

At the large-scale watershed scale, CO_2 production and emission processes are more sensitively responsive to climatic and geographic changes[39]. A recent study found that precipitation and perennial permafrost degradation are the main controlling factors for the increase of CO_2 emissions from Arctic and Tibetan Plateau rivers[99]. The carbon emission effects of the two reservoirs under different geologic conditions are significantly different[24]. In this study, CO_2 showed a significant positive correlation ($p<0.05$) with temperature (T_a), altitude (Alti) and precipitation (Precip), and Alti and Precip together explained the higher CO_2 variance (38.8%). The altitude of the upper Yellow River decreases rapidly along the course of the river, and the vegetation cover, land use, and population density of the watershed vary widely, and the CO_2 emission is significantly affected by Alti[35]. In addition, spatial differences in T_a alter carbon metabolic processes in aquatic ecosystems[10,100]. At higher elevations, lower T_a suppresses the respiratory metabolism of organisms in the water column and sediments, resulting in lower CO_2 concentrations in the water column[101]. CO_2 release from soil respiration from land-based sources enters the reservoir through surface runoff formed by rainfall, contributing to CO_2 discharge[29,102]. In conclusion, the three reservoirs in UYR have a steep top-down elevation drop, a gradual increase in temperature, and a corresponding increase in precipitation, which dominate the spatial variation of CO_2 emissions by regulating wate-land carbon metabolism and increasing exogenous carbon inputs.

(2) CH_4 emissions

Temperature (T_a, T_w) and precipitation (Precip) are critical factors that influence CH_4 emissions in rivers and reservoirs[103,104]. Temperature affects CH_4 emissions from surface waters indirectly by moderating water temperature and influencing the leaching effects of precipitation. In rivers and reservoirs, the habitat characteristics of longitudinal transport and vertical mixing impart an open character to the water temperature, resulting in significant variances in localized biogeochemical processes compared with those in closed water bodies such as lakes. In these environments, rising temperatures lead to increased water temperatures, which subsequently stimulate microbial activity, increase in situ methanogenic processes, increase oxygen consumption, and contribute to the release of CH_4 from surface water into the atmosphere[98,105]. These observations accounted for the significant positive correlations ($p<0.05$) between CH_4 and T_a and T_w in this study. Furthermore, similar to the CO_2 process, the significant positive correlation ($p<0.01$) between CH_4 and Precip indicated that precipitation carries CH_4 and exogenous organic matter from the surrounding soils into water bodies (Fig. 12)[64,106]. However, heavy rainfall events, such as storms and floods, may dilute the CH_4 concentrations in water bodies, potentially leading to opposite effects on CH_4 emissions[76,107,108].

Effects of damming on CO_2 and CH_4 emissions

Damming has profound and complex effects on the physico-chemical characteristics of rivers and associated carbon biogeochemical processes[64,109]. Contrary to the traditional perception that "the first reservoir has the highest carbon emission"[64,103,110]the present study found that the downstream LJXX reservoir contributes 67.5% of the carbon emission of the whole river section. This anomalous spatial distribution was associated with two major mechanisms: first, the LYX deep reservoir inhibited carbon sequestration by phytoplankton due to low oxygen, resulting in a special pattern of "low Chl-a and high CO_2"($p<0.01$, Table S5); and second, the LJXX was driven by pollution inputs from urbanised tributaries, and its CH_4/CO_2 flux ratio of 1.58 (only 0.29 for LJXX), indicating that gradient development significantly altered the natural metabolic pattern of the river, shifting the carbon release pattern from CO_2-dominated to CH_4-dominated. Therefore, reservoirs' own geo-environmental characteristics have a significant effect on CO_2 emissions, as well as reservoir siltation and tributary pollution on CH_4 emissions, and the effect of damming on carbon gas emissions may be more controlled by the role of environmental pressure. This provides a new idea for precise GHG emission reduction from reservoirs in the alpine region, and focusing on controlling downstream eutrophication reservoirs during the thawing period is expected to suppress CO_2 and CH_4 emissions simultaneously.

Conclusion

This study systematically reveals the seasonal characteristics of carbon GHG emissions from the water bodies of three large reservoirs in the upper Yellow River on the Tibetan Plateau and elucidates their environmental control mechanisms. It was found that all three reservoirs were net emitters of CO_2 and CH_4 during the observation period, with the soil thawing period identified as the critical window for carbon emissions, closely related to their metabolic processes. Further investigations demonstrated that carbon emissions during the freezing period were predominantly influenced by the photodegradation of organic carbon, whereas the thawing period exhibited a mixed metabolic pattern characterized by microbial anaerobic respiration, supplemented by photodegradation. In terms of environmental controls, CO_2 emissions are primarily regulated by natural geographic factors, such as altitudinal gradients and precipitation intensity, while CH_4 emissions are associated with anthropogenic activities, including the degree of sedimentation in reservoirs and pollution loads in tributaries. This paper focuses on the characteristics of reservoir GHG emissions and their environmental control mechanisms during the alternation of winter and spring in high-altitude permafrost regions, and in order to more comprehensively understand its response pattern in the annual cycle of permafrost, it is necessary to expand the study to cover the observations of all seasons of the year, so as to systematically analyse the dynamics of GHG emissions.

Data availability

All data generated or analysed during this study are included in this published article and its supplementary information files.

Received: 17 March 2025; Accepted: 26 August 2025
Published online: 03 October 2025

References

1. Regnier, P., Resplandy, L., Najjar, R. & Ciais, P. The land-to-ocean loops of the global carbon cycle. *Nature* **603**, 1–10 (2022).
2. Borges, A. V. et al. Globally significant greenhouse-gas emissions from African inland waters. *Nat. Geosci.* **8**, 637–642 (2015).
3. Gao, Y. et al. Global inland water greenhouse gas (GHG) geographical patterns and escape mechanisms under different water level. *Water Res.* **269**, 122808 (2025).
4. Silverthorn, T. et al. The importance of ditches and canals in global inland water CO_2 and N_2O budgets. *Glob Chang. Biol.* **31**, e70079 (2025).
5. Zhou, T. et al. Characteristics and influencing factors of CO_2 emission from inland waters in China. *Sci. China Earth Sci.* **67**, 2034–2055 (2024).
6. Yang, Q. et al. Carbon Emissions From Chinese Inland Waters: Current Progress and Future Challenges. *J. Geophys. Res. Biogeosci.* **129**(2), e2023JG007675 (2024).
7. Drake, T., Raymond, P. & Spencer, R. Terrestrial carbon inputs to inland waters: A current synthesis of estimates and uncertainty. *Limnology Oceanogr. Lett.* **3**(3), 132–142 (2017).
8. Lauerwald, R. et al. Inland Water Greenhouse Gas Budgets for RECCAP2: 2. Regionalization and Homogenization of Estimates. *Global Biogeochem. Cycles.* **37**(5), e2022GB007658 (2023).
9. Mendonça, R. et al. Organic carbon burial in global lakes and reservoirs. *Nat. Commun.* **8**, 1694 (2017).
10. Raymond, P. A. et al. Global carbon dioxide emissions from inland waters. *Nature* **503**, 355–359 (2013).
11. Hu, M., Chen, D. & Dahlgren, R. A. Modeling nitrous oxide emission from rivers: a global assessment. *Glob. Change Biol.* **22**, 3566–3582 (2016).
12. Cui, P., Cui, L., Zheng, Y. & Su, F. Land use and urbanization indirectly control riverine CH_4 and CO_2 emissions by altering nutrient input. *Water Res.* **265**, 122266 (2024).
13. Hayes, N. M., Deemer, B. R., Corman, J. R., Razavi, N. R. & Strock, K. E. Key differences between lakes and reservoirs modify climate signals: A case for a new conceptual model. *Limnol. Oceanogr. Lett.* **2**, 47–62 (2017).
14. Harrison, J. A., Deemer, B. R., Birchfield, M. K. & O'Malley, M. T. Reservoir Water-Level drawdowns accelerate and amplify methane emission. *Environ. Sci. Technol.* **51**, 1267–1277 (2017).
15. Deemer, B. R. et al. Greenhouse gas emissions from reservoir water surfaces: A new global synthesis. *BioScience* **66**, 949–964 (2016).
16. Deemer, B. R., Harrison, J. A. & Whitling, E. W. Microbial dinitrogen and nitrous oxide production in a small eutrophic reservoir: an in situ approach to quantifying hypolimnetic process rates. *Limnol. Oceanogr.* **56**, 1189–1199 (2011).
17. Aguilera, E. et al. Methane emissions from artificial waterbodies dominate the carbon footprint of irrigation: A study of transitions in the Food–Energy–Water–Climate nexus (Spain, 1900–2014). *Environ. Sci. Technol.* **53**, 5091–5101 (2019).
18. Rosentreter, J. A. et al. Half of global methane emissions come from highly variable aquatic ecosystem sources. *Nat. Geosci.* **14**, 225–230 (2021).
19. Johnson, M. S. et al. Spatiotemporal Methane Emission From Global Reservoirs. *J. Geophys. Res. Biogeosci.* **126**(8), e2021JG006305 (2021).
20. Waldo, S. et al. Temporal trends in methane emissions from a small eutrophic reservoir: the key role of a spring burst. *Biogeosciences* **18**, 5291–5311 (2021).
21. Zhu, D. et al. Methane emissions respond to soil temperature in convergent patterns but divergent sensitivities across wetlands along altitude. *Glob. Change Biol.* **27**, 941–955 (2021).
22. Deemer, B. R. & Holgerson, M. A. Drivers of Methane Flux Differ Between Lakes and Reservoirs, Complicating Global Upscaling Efforts. *J. Geophys. Res. Biogeosci.* **126**(4), e2019JG005600 (2021).
23. Zhong, J. et al. Water depth and productivity regulate methane (CH_4) emissions from temperate cascade reservoirs in Northern China. *J. Hydrol.* **626**, 130170 (2023).
24. Wang, W. et al. Unraveling the factors influencing CO_2 emissions from hydroelectric reservoirs in karst and non-karst regions: A comparative analysis. *Water Res.* **248**, 120893 (2024).
25. Gao, Y. et al. Carbon budget and balance critical processes of the regional land-water-air interface: indicating the Earth system's carbon neutrality. *Sci. China Earth Sci.* **65**, 1–10 (2022).
26. Ran, L. et al. Riverine CO_2 emissions in the Wuding river catchment on the loess plateau: environmental controls and dam impoundment impact. *J. Geophys. Research: Biogeosciences.* **122**, 1439–1455 (2017).
27. Chen, S. et al. Agricultural land use changes stream dissolved organic matter via altering soil inputs to streams. *Sci. Total Environ.* **796**, 148968 (2021).
28. Lofton, D. D., Whalen, S. C. & Hershey, A. E. Vertical sediment distribution of methanogenic pathways in two shallow Arctic Alaskan lakes. *Polar Biol.* **38**, 815–827 (2015).
29. Johnson, M. S. et al. CO_2 efflux from Amazonian headwater streams represents a significant fate for deep soil respiration. *Geophys. Res. Lett.* **35**, 2008GL034619 (2008).
30. Fan, L. et al. Spatio-temporal patterns and drivers of CH_4 and CO_2 fluxes from rivers and lakes in highly urbanized areas. *Sci. Total Environ.* **918**, 170689 (2024).
31. Hu, B. et al. Greenhouse gases emission from the sewage draining rivers. *Sci. Total Environ.* **612**, 1454–1462 (2018).
32. Zhang, W., Li, H., Xiao, Q., Jiang, S. & Li, X. Surface nitrous oxide (N_2O) concentrations and fluxes from different rivers draining contrasting landscapes: Spatio-temporal variability, controls, and implications based on IPCC emission factor. *Environ. Pollut.* **263**, 114457 (2020).
33. Chen, B. et al. The external/internal sources and sinks of greenhouse gases (CO_2, CH_4, N_2O) in the Pearl river estuary and adjacent coastal waters in summer. *Water Res.* **249**, 120913 (2024).
34. Almeida, R. M., Pacheco, F. S., Barros, N., Rosi, E. & Roland, F. Extreme floods increase CO_2 outgassing from a large Amazonian river. *Limnol. Oceanogr.* **62**, 989–999 (2017).
35. Huang, S. et al. Characteristics and influencing factors of greenhouse gas emissions from reservoirs in the yellow river basin: A Meta-analysis. *Sci. China Earth Sci.* **67**, 2210–2225 (2024).
36. Huttunen, J. T., Lappalainen, K. M., Saarijärvi, E., Väisänen, T. & Martikainen, P. J. A novel sediment gas sampler and a subsurface gas collector used for measurement of the ebullition of methane and carbon dioxide from a eutrophied lake. *Sci. Total Environ.* **266**, 153–158 (2001).
37. Wang, X. et al. pCO_2 and CO_2 fluxes of the metropolitan river network in relation to the urbanization of chongqing, China. *JGR Biogeosciences.* **122**, 470–486 (2017).

38. Rantakari, M. & Kortelainen, P. Interannual variation and Climatic regulation of the CO_2 emission from large boreal lakes. *Glob. Change Biol.* **11**, 1368–1380 (2005).
39. Yang, X. et al. Influence of hydrological features on CO_2 and CH_4 concentrations in the surface water of lakes, Southwest china: A seasonal and mixing regime analysis. *Water Res.* **251**, 121131 (2024).
40. Zhu, L. et al. Physical and biogeochemical responses of Tibetan plateau lakes to climate change. *Nat. Rev. Earth Environ.* **6**, 284–298 (2025).
41. Mu, C. et al. Methane emissions from thermokarst lakes must emphasize the ice-melting impact on the Tibetan plateau. *Nat. Commun.* **16**, 2404 (2025).
42. Wu, Y. et al. Groundwater-derived carbon stimulates headwater stream CO_2 emission potential on the Qinghai-Tibet plateau. *Water Res.* **268**, 122684 (2025).
43. Chen, Y., Feng, J., Yuan, X. & Zhu, B. Effects of warming on carbon and nitrogen cycling in alpine grassland ecosystems on the Tibetan plateau: A meta-analysis. *Geoderma* **370**, 114363 (2020).
44. Li, X. Y., Shi, F. Z., Ma, Y. J., Zhao, S. J. & Wei, J. Q. Significant winter CO_2 uptake by saline lakes on the Qinghai-Tibet plateau. *Glob Chang. Biol.* **28**, 2041–2052 (2022).
45. Xu, S. et al. Escalating carbon export from High-Elevation rivers in a warming climate. *Environ. Sci. Technol.* https://doi.org/10.1021/acs.est.3c06777 (2024).
46. Shang, X. et al. Riverine carbon dioxide release in the headwater region of the Qilian mountains, Northern China. *J. Hydrol.* **632**, 130832 (2024).
47. Zhang, Y. et al. Sink or source? Methane and carbon dioxide emissions from cryoconite holes, subglacial sediments, and proglacial river runoff during intensive glacier melting on the Tibetan plateau. *Fundamental Res.* **1**, 232–239 (2021).
48. Zhang, L. et al. Significant methane ebullition from alpine permafrost rivers on the East Qinghai–Tibet plateau. *Nat. Geosci.* **13**, 349–354 (2020).
49. Mu, C. et al. High carbon emissions from thermokarst lakes and their determinants in the Tibet plateau. *Glob. Change Biol.* **29**, 2732–2745 (2023).
50. Wang, J., Wu, W., Zhou, X. & Li, J. Carbon dioxide (CO_2) partial pressure and emission from the river-reservoir system in the upper yellow river, Northwest China. *Environ. Sci. Pollut Res. Int.* **30**, 19410–19426 (2023).
51. Wang, J., Wu, W., Zhou, X., Li, J. & Li, C. Distribution characteristics and sources of dissolved organic matter in the river–Reservoir system of the upper yellow river. *Environ. Eng. Sci.* **40**, 71–81 (2023).
52. Zhao, J. et al. Typical characteristics and causes of giant landslides in the upper reaches of the Yellow River, China. *Landslides* **22**(2), 313–334 (2024).
53. Liu, Y. et al. Hydrodynamics regulate longitudinal plankton community structure in an alpine cascade reservoir system. *Front. Microbiol.* **12**, 749888 (2021).
54. Miao, S. et al. Long-term and longitudinal nutrient stoichiometry changes in oligotrophic cascade reservoirs with trout cage aquaculture. *Sci. Rep.* **10**, 13483 (2020).
55. Koschorreck, M., Prairie, Y. T., Kim, J. & Marcé, R. Technical note: CO_2 is not like CH_4 – limits of and corrections to the headspace method to analyse pCO_2 in fresh water. *Biogeosciences* **18**, 1619–1627 (2021).
56. Yan, X. et al. River damming impacts on carbon emissions should be revisited in the context of the aquatic continuum concept. *Environ. Sci. Technol.* **58**, 17529–17531 (2024).
57. Benson, B. B. & Krause, D. Jr. The concentration and isotopic fractionation of oxygen dissolved in freshwater and seawater in equilibrium with the atmosphere. *Limnol. Oceanogr.* **29**, 620–632 (1984).
58. Wanninkhof, R. Relationship between wind speed and gas exchange over the ocean revisited. *Limnol. Ocean. Methods.* **12**, 351–362 (2014).
59. Wiesenburg, D. A. & Guinasso, N. L. Jr. Equilibrium solubilities of methane, carbon monoxide, and hydrogen in water and sea water. *J. Chem. Eng. Data*. **24**, 356–360 (1979).
60. Vachon, D. et al. Paired O_2–CO_2 measurements provide emergent insights into aquatic ecosystem function. *Limnol. Oceanogr. Lett.* **5**, 287–294 (2020).
61. *GHG Measurement Guidelines for Freshwater Reservoirs: Derived from: The UNESCO/IHA Greenhouse Gas Emissions from Freshwater Reservoirs Research Project* (Intern. Hydropower Association (IHA), 2010).
62. Raymond, P. A. et al. Scaling the gas transfer velocity and hydraulic geometry in streams and small rivers. *Limn Fluids Environ.* **2**, 41–53 (2012).
63. Qu, B. et al. Greenhouse gases emissions in rivers of the Tibetan plateau. *Sci. Rep.* **7**, 16573 (2017).
64. Wang, X. et al. Greenhouse gases concentrations and emissions from a small subtropical cascaded river-reservoir system. *J. Hydrol.* **612**, 128190 (2022).
65. Leng, P. et al. Deciphering large-scale Spatial pattern and modulators of dissolved greenhouse gases (CO_2, CH_4, and N_2O) along the Yangtze river, China. *J. Hydrol.* **623**, 129710 (2023).
66. Gao, S. Permafrost temperature dynamics and its climate relations in various Tibetan alpine grasslands. (2024). https://doi.org/10.1016/j.catena.2024.108065
67. Wang, M. et al. Chemical characteristics of salt migration in frozen soils during the freezing-thawing period. *J. Hydrol.* **606**, 127403 (2022).
68. DelVecchia, A. G. et al. Variability and drivers of CO_2, CH_4, and N_2O concentrations in streams across the united States. *Limnol. Oceanogr.* **68**, 394–408 (2023).
69. Wu, Z. et al. Greenhouse gas emissions (CO_2-CH_4-N_2O) along a large reservoir-downstream river continuum: The role of seasonal hypoxia. *Limnol. Oceanogr.* https://doi.org/10.1002/lno.12544 (2024).
70. Cory, R. M., Ward, C. P., Crump, B. C. & Kling, G. W. Sunlight controls water column processing of carbon in Arctic fresh waters. *Science* **345**, 925–928 (2014).
71. Torgersen, T. & Branco, B. Carbon and oxygen dynamics of shallow aquatic systems: Process vectors and bacterial productivity. *J. Geophys. Res.* https://doi.org/10.1029/2007JG000401 (2007).
72. Kai, J. et al. High thermodynamical sensitivity of CO_2 emissions from a large oligotrophic-hardwater lake (Nam Co) on the Tibetan plateau. *Sci. Total Environ.* **947**, 174682 (2024).
73. Hu, X. et al. Urban and agricultural land use regulates the molecular composition and bio-lability of fluvial dissolved organic matter in human-impacted southeastern China. *Carbon Res.* **1**, 19 (2022).
74. Smith, R. M., Kaushal, S. S., Beaulieu, J. J., Pennino, M. J. & Welty, C. Influence of infrastructure on water quality and greenhouse gas dynamics in urban streams. *Biogeosciences* **14**, 2831–2849 (2017).
75. Liu, J. et al. Strong CH_4 emissions modulated by hydrology and bed sediment properties in Qinghai-Tibetan plateau rivers. *J. Hydrol.* **617**, 129053 (2023).
76. Wang, T. et al. Time-lag effects of flood stimulation on methane emissions in the Dongting lake floodplain, China. *Agric. For. Meteorol.* **341**, 109677 (2023).
77. Ran, L. et al. Seasonal and diel variability of CO_2 emissions from a semiarid hard-water reservoir. *J. Hydrol.* **608**, 127652 (2022).
78. Maeck, A., Hofmann, H. & Lorke, A. Pumping methane out of aquatic sediments - ebullition forcing mechanisms in an impounded river. *Biogeosciences* **11**, 2925–2938 (2014).
79. Marescaux, A., Thieu, V. & Garnier, J. Carbon dioxide, methane and nitrous oxide emissions from the human-impacted Seine watershed in France. *Sci. Total Environ.* **643**, 247–259 (2018).

80. Joye, S. B., Connell, T. L., Miller, L. G., Oremland, R. S. & Jellison, R. S. Oxidation of ammonia and methane in an alkaline, saline lake. *Limnol. Oceanogr.* **44**, 178–188 (1999).
81. Qiu, S. et al. Effect of extreme pH conditions on methanogenesis: methanogen metabolism and community structure. *Sci. Total Environ.* **877**, 162702 (2023).
82. Wu, Y. et al. Microbial community abundance affects the methane ebullition flux in Dahejia reservoir of the yellow river in the warm season. *Diversity* **15**, 154 (2023).
83. Lavergne, C. et al. Temperature differently affected methanogenic pathways and microbial communities in sub-Antarctic freshwater ecosystems. *Environ. Int.* **154**, 106575 (2021).
84. Halbedel, S. & Koschorreck, M. Regulation of CO_2 emissions from temperate streams and reservoirs. *Biogeosciences* **10**, 7539–7551 (2013).
85. Larsen, S., Andersen, T. & Hessen, D. O. The pCO_2 in boreal lakes: Organic carbon as a universal predictor?. *Global Biogeochem. Cycles* https://doi.org/10.1029/2010GB003864 (2011).
86. Liu, S. et al. Global Controls on DOC Reaction Versus Export in Watersheds: A Damköhler Number Analysis.. *Global Biogeochem. Cycles*. **36**(4), e2021GB007278 (2022).
87. Liu, S. et al. Dynamic biogeochemical controls on river pCO_2 and recent changes under aggravating river impoundment: an example of the subtropical Yangtze river. *Glob. Biogeochem. Cycles*. **30**, 880–897 (2016).
88. Finlay, K., Vogt, R. J., Simpson, G. L. & Leavitt, P. R. Seasonality of pCO_2 in a hard-water lake of the Northern great plains: the legacy effects of climate and Limnological conditions over 36 years. *Limnol. Oceanogr.* **64**, S118–S129 (2019).
89. Finlay, K. et al. Decrease in CO_2 efflux from Northern Hardwater lakes with increasing atmospheric warming. *Nature* **519**, 215–218 (2015).
90. Qi, T. et al. Spatiotemporal heterogeneity of lake carbon dioxide flux leads to substantial uncertainties in regional upscaling estimates. *Sci. Total Environ.* **948**, 174920 (2024).
91. Almeida, R. M. et al. High primary production contrasts with intense carbon emission in a eutrophic tropical reservoir. *Front Microbiol* **7**, (2016).
92. West, W. E., Coloso, J. J. & Jones, S. E. Effects of algal and terrestrial carbon on methane production rates and methanogen community structure in a temperate lake sediment. *Freshw. Biol.* **57**, 949–955 (2012).
93. Chan, C. N., Shi, H., Liu, B. & Ran, L. CO_2 and CH_4 emissions from an arid fluvial network on the Chinese loess plateau. *Water* **13**, 1614 (2021).
94. Yang, M. et al. Spatial-temporal characteristics of methane emission flux and its influence factors at Miyun reservoir in Beijing. *Wetland Sci.* **9**, 191–197 (2011).
95. Yang, L. et al. Spatial and seasonal variability of diffusive methane emissions from the Three Gorges Reservoir. *J. Geophys. Res. Biogeosci.* **118**(2), 471–481 (2013).
96. Xing, Y. et al. Methane and carbon dioxide fluxes from a shallow hypereutrophic subtropical lake in China. *Atmos. Environ.* **39**, 5532–5540 (2005).
97. Conrad, R. & Rothfuss, F. Methane oxidation in the soil surface layer of a flooded rice field and the effect of ammonium. *Biol. Fertil. Soils*. **12**, 28–32 (1991).
98. Schrier-Uijl, A. P., Veraart, A. J., Leffelaar, P. A., Berendse, F. & Veenendaal, E. M. Release of CO_2 and CH_4 from lakes and drainage ditches in temperate wetlands. *Biogeochemistry* **102**, 265–279 (2011).
99. Mu, C. et al. Recent intensified riverine CO_2 emission across the Northern hemisphere permafrost region. *Nat. Commun.* **16**, 3616 (2025).
100. Lauerwald, R., Laruelle, G. G., Hartmann, J., Ciais, P. & Regnier, P. A. G. Spatial patterns in CO_2 evasion from the global river network. *Glob. Biogeochem. Cycles*. **29**, 534–554 (2015).
101. Crawford, J. T., Dornblaser, M. M., Stanley, E. H., Clow, D. W. & Striegl, R. G. Source limitation of carbon gas emissions in high-elevation mountain streams and lakes: MOUNTAIN STREAM EMISSIONS. *J. Geophys. Res. Biogeosci.* **120**, 952–964 (2015).
102. Gu, S., Xu, Y. J. & Li, S. Unravelling the Spatiotemporal variation of pCO_2 in low order streams: linkages to land use and stream order. *Sci. Total Environ.* **820**, 153226 (2022).
103. DelSontro, T., Perez, K. K., Sollberger, S. & Wehrli, B. Methane dynamics downstream of a temperate run-of-the-river reservoir. *Limnol. Oceanogr.* **61**, S188–S203 (2016).
104. Li, T. et al. Methane emissions from wetlands in China and their climate feedbacks in the 21st century. *Environ. Sci. Technol.* **56**, 12024–12035 (2022).
105. Avery, G. B., Shannon, R. D., White, J. R., Martens, C. S. & Alperin, M. J. Controls on methane production in a tidal freshwater estuary and a peatland: methane production via acetate fermentation and CO_2 reduction. *Biogeochemistry* **62**, 19–37 (2003).
106. Yu, Z. et al. Carbon dioxide and methane dynamics in a human-dominated lowland coastal river network (Shanghai, China). *J. Geophys. Research: Biogeosciences*. **122**, 1738–1758 (2017).
107. Liao, Y. et al. Large methane emission from the river Inlet region of eutrophic lake: A case study of lake Taihu. *Atmosphere* **14**, 16 (2022).
108. Sawakuchi, H. O. et al. Methane emissions from Amazonian rivers and their contribution to the global methane budget. *Glob Chang. Biol.* **20**, 2829–2840 (2014).
109. Meybeck, M. Global analysis of river systems: from Earth system controls to anthropocene syndromes. *Philos. Trans. R Soc. Lond. B Biol. Sci.* **358**, 1935–1955 (2003).
110. Shi, W. et al. Carbon emission from cascade reservoirs: Spatial heterogeneity and mechanisms. *Environ. Sci. Technol.* **51**, 12175–12181 (2017).

Acknowledgements

This study was financially supported by the Joint Funds of the National Natural Science Foundation of China (No. U2243242).

Author contributions

Chen Li: Investigation, Software, Visualization, Writing – original draft. Wei Wu: Conceptualization, Methodology, Writing – original draft, Funding acquisition. Hang Chen: Software, Writing – review & editing, Project administration. Lei Ren: Methodology, Data curation. Xiao Kang: Conceptualization, Writing – review & editing, Supervision.

Declarations

Competing interests

The authors declare no competing interests.

Additional information

Supplementary Information The online version contains supplementary material available at https://doi.org/10.1038/s41598-025-17745-0.

Correspondence and requests for materials should be addressed to W.W.

Reprints and permissions information is available at www.nature.com/reprints.

Publisher's note Springer Nature remains neutral with regard to jurisdictional claims in published maps and institutional affiliations.